Taphonomy and evolution of Lower Jurassic lithiotid bivalve accumulations in the Apennine Carbonate Platform (southern Italy)

Renato Posenato [a, *], Davide Bassi [a], Alberto Trecalli [b], Mariano Parente [b]

[a] *Dipartimento di Fisica e Scienze della Terra, Università degli Studi Ferrara, via Saragat 1, 44122 Ferrara, Italy*

[b] *Dipartimento di Scienze della Terra, dell'Ambiente e delle Risorse, Università degli Studi di Napoli "Federico II", Largo S. Marcellino 10, 80138 Napoli, Italy*

* Corresponding author.

E-mail addresses: psr@unife.it (R. Posenato), bsd@unife.it (D. Bassi), etneo82@gmail.com (A. Trecalli), maparent@unina.it (M. Parente).

ABSTRACT

Lower Jurassic Tethyan and Panthalassan marine shallow-water successions are characterized by aberrant lithiotid bivalves belonging to the *Lithiotis* Fauna. Their widespread occurrence, often in rock-forming abundance, represents a global biofacies, mostly restricted to the Pliensbachian–early Toarcian. Despite their wide occurrence and their prominent role as carbonate producers in shallow-water platforms, the biogeographic and stratigraphic distribution of this group of bivalves and their evolutionary history are obscure, mostly because the identification at lower taxonomical rank (generic or specific level) was frequently missed. In particular, their evolution and demise in relation to important events of global palaeoenvironmental perturbations, like the Pliensbachian-Toarcian boundary event and the early Toarcian oceanic anoxic event are not yet known in detail. In the Apennine Carbonate Platform of southern Italy, the *Lithiotis* Member, in the upper part of the Lower Jurassic *Palaeodasycladus* Limestones Formation, is characterized by the abundant occurrence of lithiotid bivalves. They disappear abruptly in the lowermost beds of the overlying Oolitic-oncolitic Limestones Formation, at the onset of the early Toarcian Oceanic Anoxic Event. More than 60 lithiotid bivalve concentrations occur in a nearly 120 m-thick succession spectacularly exposed on freshly cut walls in a quarry west of Mercato San Severino (Salerno). Field observations on taxonomic composition and fabric of shell beds (packing, maximum shell size, degree of shell articulation and fragmentation) allowed distinguishing four tapho-horizons (A-D).

Tapho-horizon A records the appearance and spreading of the lithiotids, with accumulations characterized mainly by small-sized and loosely packed shells. Tapho-horizon B records the acme of lithiotid bivalves, with densely packed accumulations of large shells. These two tapho-horizons yield prevailing articulated individuals, frequently in life position. Tapho-horizon C records a decrease of the shell packing and frequency of articulated shells. However, it is not clear if this represents the beginning of a prolonged crisis or just the local response to less favourable

environmental conditions around a sequence boundary zone. Tapho-horizon D consists of three shell beds, one in the uppermost part of the *Lithiotis* Member and two within the lowermost part of the Oolitic-oncolitic Limestones Formation, in the stratigraphic interval characterized by the negative carbon isotope excursion of the early Toarcian OAE. The bivalve shells of these two beds consists exclusively of disarticulated and fragmented shells, possibly reworked from underlying levels.

The demise of the lithiotids carbonate factory in the Apennine Carbonate Platform and the extinction of the largest aberrant bivalves of the *Lithiotis* fauna at the onset of the early Toarcian anoxic event was probably due to physiological stress imposed by ocean acidification and increased nutrient input.

Keywords:

Bivalves; taphonomy; carbonate platforms; T-OAE; Lower Jurassic; Apennines

78 **1. Introduction**

79

80 In Tethyan and Panthalassan marine shallow-water and lagoonal settings, the Early Jurassic is
81 characterized by the appearance and diffusion of large (up to 50–70 cm high) and aberrant bivalves
82 known as lithiotids (e.g., Broglio Loriga and Neri, 1976; Geyer, 1977; Leinfelder et al., 2002;
83 Fraser et al., 2004; Posenato and Masetti, 2012). These bivalves mostly consist of semi-infaunal,
84 sessile, stick-like or spoon-shaped shells, represented by *Lithiotis*, *Cochlearites* and *Lithioperna*,
85 whose evolutionary origin and systematics is still obscure. The lithiotid accumulations make up
86 sedimentary bodies of variable thickness and shape. The lens-shaped shell accumulations, or
87 bivalve mounds, reached about 3–5 m in height and several hundred metres width (e.g., Bosellini
88 1972; Scheibner and Reijmer, 1999; Posenato and Masetti, 2012). Lithiotids had a very important
89 role as carbonate producers in shallow-marine environments due to their large-sized shells,
90 gregarious habit, and sediment-trapping efficiency.
91 The precise appraisal of the stratigraphic distribution of lithiotid bivalves, in particular of their
92 appearance and extinction, is hindered by the difficulties of their taxonomic identification in the
93 field, because the shells generally occur embedded in hard indurated limestones. For this reason, in
94 the geologic literature many citations of lithiotids refer to Lower Jurassic accumulations of
95 undetermined bivalves, often not illustrated. In the western Tethyan shallow-water sedimentary
96 successions for which a reliable stratigraphic information is available, the maximum lithiotid
97 diffusion occurred in the late Pliensbachian, when the group attained a relevant ecological role in
98 the carbonate platform dynamics (e.g., Leinfelder et al., 2002; Posenato & Masetti, 2012). The
99 demise of the lithiotid bivalve carbonate factory occurred in the early Toarcian and has been related
100 to the environmental changes connected with the oceanic anoxic event (e.g., Fraser et al., 2004;
101 Trecalli et al., 2012; Posenato and Masetti, 2012; Sabatino et al., 2013).
102 Despite the global distribution of the lithiotid facies, detailed information on the stratigraphic
103 distribution of lithiotid genera, the geometry of their shell accumulations and their sedimentary

104 role is only available for a few areas. Most of the available information refers to the lithiotids of the
105 Rotzo Formation from the Trento Platform (Southern Alps, Italy; e.g., Posenato and Masetti, 2012;
106 Franceschi et al., 2014). In this paper, we present taxonomic and taphonomic data on a lithiotid-
107 bearing succession of the Apennine Carbonate Platform (ACP), southern Italy (Fig. 1). In this area,
108 the occurrence of *Lithiotis problematica* and other large lithiotids has been reported in the Monti
109 Lattari, Monti Picentini and Capri Island (Napoli and Salerno provinces; e.g., De Castro, 1962). The
110 occurrence of *Lithioperna* and *Cochlearites* has been also recorded (Broglio Loriga and Neri, 1976;
111 Accorsi Benini, 1979), but detailed studies on the systematics, stratigraphic distribution and
112 geometry of lithiotid accumulations are missing. A thick Lower Jurassic sedimentary succession of
113 the ACP, with several lithiotid-bearing beds (*Lithiotis* Facies in De Castro, 1962; *Lithiotis* Member
114 of the *Palaeodasycladus* Limestones Formation in Catenacci et al., 1963) has been recently
115 investigated to define the response of the platform to the early Toarcian Oceanic Anoxic Event (T-
116 OAE; Trecalli et al., 2012). A precise chronostratigraphic calibration for this succession, which is
117 spectacularly exposed in an active quarry (Maiellaro Quarry) near Mercato San Severino (11 km
118 north of Salerno; Fig. 2), has been achieved by integrating carbon isotope stratigraphy and
119 biostratigraphy (Trecalli et al., 2012). The *Lithiotis* Member, which in this quarry is about 120 m
120 thick, overlies grey limestones with scattered megalodontid shells and is followed by the Toarcian
121 Oolitic-oncolitic Limestones Formation, almost barren in mollusc remains. The fresh cuts of the
122 quarry walls allow a good observation of the lithiotids and their taxonomic identification at the
123 genus level. Therefore, the continuous, thick and well exposed succession of the Maiellaro Quarry
124 represents a key section to investigate the evolution of lithiotid bivalves in the ACP. This paper
125 investigates the appearance, flourishing and demise of the lithiotids by analysing in detail the
126 taxonomic composition, fabric and taphonomy of shell accumulations. The results are then
127 compared with the Trento Platform coeval counterpart and are used to explore the relations between
128 the evolution and demise of the lithiotid facies and the palaeoenvironmental perturbations linked to

129 the Pliensbachian–Toarcian (P-To) boundary event (Littler et al., 2010; Suan et al., 2010) and to the
130 T-OAE (e.g., Jenkyns, 1988; Hesselbo et al., 2000, 2007; Hermoso et al., 2012).
131
132 **2. Stratigraphic setting**
133
134 The ACP is made of a 4–5 km thick pile of Upper Triassic–Upper Cretaceous shallow-water
135 carbonates deposited at the southern margin of the Tethyan Ocean (Bosellini, 2004; Fig. 1). The
136 Lower Jurassic interval of the ACP succession comprises the *Palaeodasycladus* Limestones
137 Formation, named after its more distinctive fossil, the dasycladalean alga *Palaeodasycladus*
138 *mediterraneus*. In the upper part of the *Palaeodasycladus* Limestones Formation, represented by the
139 *Lithiotis* Member, lithiotid bivalves are the main biogenic component together with dasycladalean
140 algae. The *Palaeodasycladus* Limestones Formation is overlain by the Oolitic–oncolitic Limestones
141 Formation, through a very sharp boundary corresponding to the sudden disappearance of the
142 lithiotid bivalves and of *P. mediterraneus* (Trecalli et al., 2012).
143 The *Lithiotis* Member and the overlying Oolitic-oncolitic Limestones Formation are
144 spectacularly exposed in the Maiellaro Quarry (Figs 2, 3). The lithiotid-rich interval is about 120 m
145 thick. It consists of metre-thick lithiotid accumulations, alternating with algal-peloidal-intraclastic
146 grainstones and rudstones rich of *P. mediterraneus*, which often represent the total dominant
147 component (Fig. 4). The limestone beds are often capped by mm- to cm-thick discontinuous green
148 marls, which infiltrate downward in a complex network of irregular cavities. Thicker green marly
149 levels (up to 20 cm thick), alternating with decimetric-thick beds of ostracod-charophycean
150 mudstones–wackestones, makes two distinct clusters at about 80 m and at about 110 m from the
151 base of the studied succession. These green marls have been linked to ephemeral subaerial exposure
152 of the platform top (Trecalli et al., 2012), in analogy with the "Purbeckian" green marls of Jura
153 Mountains (Strasser, 1988). The thicker marls, alternating with restricted marine to paralic
154 ostracod-charophycean mudstones-wackestones, have been interpreted as recording longer and

155 closely recurrent phases of subaerial exposure around sequence boundary zones (*sensu* Strasser et
156 al., 2000). The uppermost interval of the *Lithiotis* Member is also characterised by thinner and less
157 recurrent bivalve biostromes and by an overall shift to mud-dominated facies (Trecalli et al., 2012).
158
159 **3. Material and methods**
160
161 The bivalves of the *Lithiotis* Member in the Maiellaro Quarry cannot be isolated from the rock
162 because the shells occur in hard indurated limestone. The taxonomic identification and taphonomic
163 analysis can be performed, therefore, only on randomly sectioned shells observable on the quarry
164 walls. This type of shell exposures allows the taxonomic identification only of those specimens
165 sectioned along planes showing the diagnostic characters. In the stick-like shells, the sections with
166 taxonomic relevance are generally those passing transversally the umbonal region (e.g., Chinzei,
167 1982).
168 The taxonomic and taphonomic data were recorded in the field and from photographic surveys
169 of the studied outcrops. During the first phase of field work, carried out in 2009 and 2010, the
170 succession was logged and sampled (bed-by-bed) and field macro-photographs of surfaces oriented
171 nearly perpendicular to bedding were taken. During the second phase of the field work, carried out
172 in 2014, a detailed taxonomic and taphonomic investigation of the shell beds was performed only in
173 the lower and middle part of the succession. The data for the uppermost part of the succession
174 (around the boundary between the *Lithiotis* Member and the Oolitic-oncolitic Limestones
175 Formation), which was no longer accessible due to quarrying operations, were obtained from the
176 macro-photographs taken during the first phase of the field work. The comparison of data collected
177 on the field and from macro-photographs of the same bed indicates that both methods provide
178 reliable taxonomical and taphonomic information.
179 The typical bivalves of the *Lithiotis* Fauna are represented by three monospecific genera,
180 characterized by large, stick- or spoon-shaped shells, which developed a mud-sticker strategy of

soft-bottom stabilization (Seilacher, 1984). They are *Lithiotis*, *Cochlearites*, and *Lithioperna*, which have the most relevant role in the production of the Pliensbachian shell beds. These bivalves are also collectively referred to as "lithiotids" in the geological literature, a term with no taxonomic value. The genus-level classification used in this paper follows the descriptions and illustrations reported in the literature (e.g., Berti Cavicchi et al., 1971; Accorsi Benini and Broglio Loriga, 1977, 1982; Chinzei, 1982; Broglio Loriga and Posenato, 1996; Debeljak and Buser, 1998; Fraser et al., 2004; Posenato and Masetti, 2012; Posenato et al., 2013).

For each lithiotid accumulation, the maximum shell size was measured and the shell packing (packing index, PI), articulation (articulation index, AI) and fragmentation (fragmentation index, FI) were semi-quantitatively estimated from field macro-photographs. Each index, ranging in value from 1 to 4, covers four categories distinguished by percent-surface (PI)/percent-occurrence (AI)/percent-occurrence (FI) shells as to < 25% (value 1), 25–50% (value 2), 50–75% (value 3) and >75% (value 4) respectively (Fig. 5; see Tab. 1, supplementary material). This semi-quantitative method follows the Kidwell and Holland's (1991) approach.

The value of each index was multiplied for the shell-bed thickness to calculate a thickness-weighted score representing the relative contribution of each shell bed to the whole succession. For instance, the thickness-weighted packing score of a 50 cm-thick shell bed with a packing index of 4 is 200.

Four tapho-horizons were distinguished based on the changes in taxonomic composition and taphonomic characters of the bivalve shell-beds. For each tapho-horizon, the horizon-averaged packing, articulation and fragmentation scores were calculated by summing the values of the thickness-weighted scores of each shell-bed and dividing the sum by the total thickness of the horizon. The horizon-averaged packing score is used as a proxy of the rock-building contribution of the lithiotid bivalves, because it embodies information on the lithiotid abundance relative to the total volume of the rock. Finally, the maximum and average values of the larger shell size for each tapho-horizon was also determined (see Tab. 2, supplementary material).

207

208 *3.1. Taxonomic identification and distribution of lithiotid bivalves*

209

210 *Lithiotis* is characterized by strongly asymmetrical valves. Transversal sections of the umbonal
211 region of the thicker valve are easily distinguishable for the sub-trapezoidal outline and for the
212 presence of umbonal cavities in the dorsal region of the body cavity (e.g., Chinzei, 1982, fig. 2).
213 Specimens dubitatively attributed to this genus occur in the upper part of the *Lithiotis* Member (Fig.
214 9B) and in the lowermost part of Oolitic-oncolitic Limestones Formation (Fig. 6F).
215 *Cochlearites* is characterized by transversal sections of the umbonal region with a median
216 internal furrow on the thicker (left) valve and a median internal ridge on the thinner (right) valve
217 (e.g. Chinzei, 1982, fig. 3; Fig. 6J). It is very abundant in the Maiellaro quarry, especially in the
218 middle and upper part of the *Lithiotis* Member (Fig. 7). This bivalve occurs frequently in life
219 position, making up locally bouquet-like aggregates (Fig. 6D).
220 *Lithioperna* has large and flattened shells that resemble, in transversal section, a couple of
221 nearly equidimensional lenses, sometimes with an asymmetrical small and rounded inner cavity
222 corresponding to the anterior, cone-like extension of body cavity (Figs. 6A–B). This genus has a
223 wide stratigraphic distribution in the studied succession (Fig. 7).
224 In the Southern Alps, Lower Jurassic bivalve accumulations sometimes can be originated by
225 other bivalve genera, both with a byssate or recliner mode of life (e.g., Broglio Loriga and Neri,
226 1976). These byssate bivalves are represented by *Mytiloperna* and *Gervilleioperna*, respectively
227 characterized by sub-equivalve and inequivalve shells. The former genus has a mytiliform shell
228 with a very thick dorsal region, where it shows a massive triangular transversal section with an
229 anterior inner small cavity corresponding to the cone-like extension of body cavity (e.g., Broglio
230 Loriga and Posenato, 1996; figs. 5 G–I). *Mytiloperna* shells are very common and have a wide
231 stratigraphic distribution in the Maiellaro quarry (Fig. 7). They are mostly represented by
232 articulated shells, about 10 cm in size (Figs 6C, H, 9A). No specimen of *Gervilleioperna* was

identified in the studied succession.

The edgewise recliner *Opisoma*, with the typical moustache-like outline of the hinge region in transversal section (Posenato et al., 2013, fig. 4), shows scattered occurrence in the Maiellaro quarry (Figs. 6K, 7). Other edgewise recliners are represented by megalodontids, which show a thick shell with the typical subtriangular to heart-like outline in cross sections (Fig. 6G). They are common in the whole succession, although they do not form significant shell concentrations. The distinction between the most common Lower Jurassic megalodontids such as *Protodiceras*, *Pachyrisma* (*Durga*) and *Pachyrisma* (*Pachymegalodon*) (e.g., Accorsi Benini and Broglio Loriga, 1982) was not possible by means of random shell sections as they occur in the studied hard indurated limestone. Sparse occurrences of megalodontids were also noted in the lower part of the Maiellaro quarry succession, before the appearance of the lithiotids.

4. Results

4.1. Taphonomy of the bivalve shell-beds

Four tapho-horizons were distinguished based on variations in the taphonomic characters of the shell beds (i.e., packing/articulation/fragmentation indexes, mean value of maximum shell size; Figs. 7, 8). All the bivalve accumulations show a tabular shape (biostrome) at the scale of observation permitted by the studied outcrop, which exposes each bed for up to a few tens of meters.

The lower tapho-horizon A is about 35 m thick and its base is characterised by the appearance of the lithiotid accumulations. The cumulative thickness of the bivalve accumulations (715 cm) is about 20% of the total horizon thickness. The horizon-averaged PI is 0.44, the AI is 0.52 and the FI is 0.48. The mean value of the maximum shell size is 14 cm and the largest value is 30 cm. Bivalve biostromes of the tapho-horizon A are dominated by *Mytiloperna. Lithioperna*

appears at about 8 m above the horizon base. *Cochlearites* is rare and was recognized only in one accumulation, located at about 25 m above the base.

The tapho-horizon B, about 50 m thick, corresponds to the interval with the greatest frequency of lithiotid accumulations, the highest PI and the maximum shell size. The horizon-averaged PI (1.15) and AI (1.02) show a remarkable increase with respect to those of the underlying horizon. The maximum shell size shows a mean value of 20 cm, with the largest size (60 cm) recorded by individuals of *Cochlearites*, arranged in a bouquet-like cluster (Fig. 6D). The shell accumulations of this interval consist mostly of *Cochlearites*, predominantly represented by articulated shells, often in life position. *Mytiloperna* and *Lithioperna* are abundant. The cumulative thickness of the bivalve accumulations (1,980 cm) is more than 40% of the whole tapho-horizon B thickness.

The tapho-horizon C, about 35 m thick, records a marked decrease in shell size and frequency. The cumulative shell-bed thickness is more than 40% of the whole interval thickness. However, the cumulative PI is about half that of the underlying tapho-horizon B. The mean value of maximum shell size (16 cm) and the horizon-averaged PI (0.70) and AI (0.67) drop significantly (Fig. 8).

The tapho-horizon D, about 7 m thick, is characterized by fragmented and possibly reworked shells. The lower limit of this tapho-horizon has been placed at the first accumulation containing only fragmented shells (Fig. 7). This accumulation is located at about 5 m below the *Lithiotis* Member/Oolitic-oncolitic Limestones Formation boundary, corresponding to the onset of the carbon isotope excursion of the early T-OAE (Trecalli et al., 2012). The lithiotid accumulations are characterized by the absence of articulated shell and by a very low horizon-averaged PI (0.10). Noteworthy is the occurrence of some broken shells that could be dubitatively referred to the genus *Lithiotis* (Fig. 6F).

5. Discussion

285

286 *5.1. Comparing the Lithiotis Member of southern Apennines with the Rotzo Formation of the Trento*
287 *Platform*

288

289 A large part of the current knowledge on the biostratigraphy, taphonomy and palaeoecology
290 of the Lower Jurassic lithiotid bivalves has been derived from the classical outcrops of the Rotzo
291 Formation in the Trento Platform (Southern Alps, Italy), which have been the topic of
292 palaeontological and sedimentological investigations since the 19th century (e.g., Gümbel, 1871;
293 Reis, 1903; Bosellini, 1972; Accorsi Benini and Broglio Loriga, 1977; Chinzei, 1982; Fraser et al.,
294 2004; Posenato and Masetti, 2012; Franceschi et al., 2014). In the Trento Platform, *Cochlearites*
295 spreads in the upper part of Rotzo Formation (*Lituosepta compressa* zone, late Pliensbachian;
296 Fugagnoli, 2004; Posenato and Masetti, 2012), within prevailing meso-eutrophic marine conditions
297 (Fugagnoli, 2004). *Mytiloperna* is common in the lower Rotzo Formation, where it is associated
298 with *Gervilleioperna* and *Pseudopachymytilus*. This association has been considered indicative of a
299 shallow subtidal environment (Accorsi Benini and Broglio Loriga, 1982). *Lithioperna* ranges
300 throughout the whole Rotzo Formation, with abundance peaks at different stratigraphic levels and
301 localities, related to local environmental factors. *Opisoma* shows the maximum abundance in
302 shallow marine environments near the platform margin, in association with benthic organisms (e.g.,
303 brachiopods) typical of fully marine euhaline conditions (Posenato et al., 2013). *Lithiotis* is also
304 often associated with abundant brachiopods and larger foraminifera, indicating slightly deeper
305 marine conditions (Fraser et al., 2004; Posenato and Masetti, 2012).
306 Compared to the Rotzo Formation, the *Lithiotis* Member of the Maiellaro quarry shows a
307 quite remarkable overall stability of palaeoenvironmental conditions. The only significant facies
308 change occurs in the uppermost part of the studied succession, where there is a shift to more muddy
309 facies with thicker interlayers of nodular marls and less frequent and thinner bivalve biostromes.
310 The lithiotid accumulations of the Maiellaro Quarry are dominated by *Cochlearites* and

311 *Mytiloperna* with subordinated *Lithioperna*. *Opisoma* and *Lithiotis* occurrences are more scattered.
312 Most of the bivalve accumulations contain still articulated shells, often in life position, which
313 indicates a high rate of sediment accumulation (e.g., Kidwell, 1991; Hauser et al., 2008). The high
314 abundance of *Mytiloperna* suggests a very shallow marine environment, supported also by the great
315 abundance of the dasycladalean alga *P. mediterraneous,* which is instead uncommon in the Rotzo
316 lagoon of the Trento Platform.
317 In the *Lithiotis* Member of the Maiellaro Quarry, the tabular shape of the bivalve
318 accumulations could be related to a slower subsidence rate and to a more flat and oxygenated sea
319 bottom of this sector of the ACP compared to the Trento Platform, where upper Pliensbachian lens-
320 shaped accumulations (bivalve mounds) record episodes of restricted circulation and recurrent
321 dysaerobic conditions (Posenato and Masetti, 2012).
322 The different subsidence rate, water depth and oxygen level probably determined the
323 different evolution of the two platforms during the late Pliensbachian–Toarcian. The Trento
324 Platform shows a shift to more clay-rich facies during the T-OAE, recording a long-term decrease
325 of carbonate production that probably preconditioned the platform to its definitive drowning in the
326 middle Jurassic (Woodfine et al., 2008). In the southern Apennines, although the carbonate
327 production shifted from biotic (lithiotid bivalves and calcareous green algae) to chemical (oolites) at
328 the onset of the event, the shallow-water platform was able to keep pace with subsidence (Trecalli
329 et al., 2012).
330 Considering the Rotzo Formation as a biostratigraphic reference for the *Lithiotis* Member of
331 the Maiellaro succession, the abundance of *Cochlearites* and the absence of *Orbitopsella* suggest a
332 late Pliensbachian–early Toarcian age, as already proposed by Trecalli et al. (2012). A late
333 Pliensbachian age for the base of the *Lithiotis* Member is also supported by the absence, in the
334 lower part of the succession, of the remarkable $\delta^{13}C$ perturbations, which mark the Sinemurian–
335 Pliensbachian boundary and the lower Pliensbachian in the Trento Platform (Franceschi et al.,
336 2014).

337

338 *5.2. The demise of the western Tethyan lithiotid bivalves: sudden or prolonged crisis?*

339

340 The uppermost part of the studied *Lithiotis* Member is characterized by the increasing
341 frequency and thickness of marly interlayers and by an overall shift to more muddy facies (Trecalli
342 et al., 2012). This part corresponds to the upper tapho-horizon C, characterised by both sparse and
343 dense lithiotid accumulations with abundant *Mytiloperna* and *Cochlearites*. In some beds, these
344 bivalves make up dense accumulations with articulated and large shells still in life position (e.g., 30
345 cm-large ?*Cochlearites* shells; Fig. 9 B). These dense accumulations of articulated shells occur up
346 to 10 m below the base of the Oolitic-oncolitic Limestones Formation. Overall, the tapho-horizon C
347 records a marked decrease of both average PI and AI, compared to the underlying tapho-horizon B
348 (Fig. 8). The decrease of the PI points to bottom conditions less favourable to the bivalves, while
349 the decrease of the AI could be related to a drop of the sedimentation rate. Carbon and strontium
350 isotope stratigraphy suggests that this interval spans from the Pliensbachian–Toarcian boundary (P-
351 To boundary) into the earliest Toarcian (Trecalli et al., 2012). A crisis of neritic carbonate
352 production around the P-To boundary is recorded in many Tethyan carbonate platforms (e.g.,
353 Bassoullet and Baudin, 1994). Increased nutrient delivery to coastal areas under accelerated
354 weathering and continental hydrological cycling, ultimately driven by global warming, have been
355 invoked as the main cause of the crisis (Cohen et al., 2004; Dera et al., 2009; Bodin et al., 2010;
356 Suan et al., 2010; Krenker et al., 2015). Many Tethyan platforms did not survive the crisis and
357 drowned (Blomeier and Reijmer, 1999; Wilmsen and Neuweiler, 2008; Léonide et al., 2012). In the
358 ACP, the P-To boundary interval was characterized by the repeated occurrence of restricted marine
359 to paralic conditions and by longer and closely recurrent phases of subaerial exposure (Trecalli et
360 al., 2012). The decrease in carbonate production could be due to palaeoenvironmental conditions
361 less favourable to lithiotid bivalves during an interval of low sea-level. More global causes of
362 palaeoenvironmental perturbation, like increased nutrient input, could also have played a role. In

any case, the ACP was able to survive in shallow-water.

Following this interval, the overlying tapho-horizon D comprises three accumulations with sparse and fragmented bivalve shells. Some of the shell fragments are dubitatively assigned to the genus *Lithiotis*, while others could not be identified (Fig. 7). The second and third shell accumulations of tapho-horizon D occur within the lowermost part of the Oolitic-oncolitic Limestones Formation, in the stratigraphic interval characterized by the negative carbon isotope excursion of the T-OAE (Trecalli et al., 2012; Fig. 7). The bivalve shells of these accumulations are exclusively disarticulated and fragmented, suggesting a possible reworking from underlying levels (Fig. 6F).

Summing up, the detailed taxonomic and taphonomic study of the lithiotid bivalve accumulations of the Maiellaro quarry showed that:

1) Lithiotid bivalves attained their maximum abundance and size in the tapho-horizon B, in the middle part of the *Lithiotis* Member.
2) A decrease of the rock-building contribution of lithiotid bivalves, evidenced by a decrease in packing and articulation indexes, is already recorded in the tapho-horizon C, well below the onset of the negative T-OAE carbon-isotope excursion. However, it is not clear if this decrease represents the beginning of a prolonged crisis, or just the local response to less favourable environmental conditions, as speculated by Trecalli et al. (2012).
3) The last beds with bivalves occurs within the Oolitic-oncolitic Limestone Formation, but they are represented only by fragmented and abraded, possibly reworked, shells.

The early Toarcian biotic extinction has been related to global warming, high nutrient input, anoxia and ocean acidification (Harries and Little, 1999; Pálfy and Smith, 2000; Jenkyns, 2003; Wignall et al., 2005; Kiessling and Simpson, 2011; Hönisch et al., 2012; Trecalli et al., 2012; Caswell and Coe 2013, 2014). In such a scenario, opportunistic bivalves (e.g., *Pseudomytiloides dubius*) show a surviving strategy represented by body size reduction (i.e., Lilliput effect;

389 Urbanek, 1993; Twitchett, 2007; Morten and Twitchett, 2009), short life cycle and high recruitment
390 rate (Caswell and Coe, 2013). Other bivalves, better adapted to dysaerobic environments, such as
391 *Bositra* (e.g., Allison et al., 1995) show an inverse behaviour. Their shell size and abundance
392 increase immediately before and after the extinction interval, because of their greater capability of
393 exploiting the rising of primary productivity.
394 Out of the six genera traditionally included in the lithiotids, *Lithiotis*, *Cochlearites* and
395 *Lithioperna* were affected by the early Toarcian extinction while *Gervilleioperna*, *Mytiloperna* and
396 *Opisoma* also occur in the Middle and Late Jurassic (e.g., Aberhan and Hillebrandt, 1996; Yin and
397 Fürsich, 1991). This pattern suggests that two forcing factors led to the selective extinction of the
398 most aberrant and the largest Pliensbachian bivalves. One possible forcing factor was the increased
399 nutrient input to coastal areas: *Lithiotis*, *Cochlearites* and *Lithioperna*, with their extraordinarily
400 large shells (from 30 to 70 cm; e.g., Debeljak and Buser, 1997), were doomed to extinction because
401 they were adapted to meso-oligotrophic environments (Fugagnoli, 2004; Franceschi et al., 2014).
402 Another forcing factor was the stress imposed by a transient reduction of carbonate saturation state
403 of the ocean, which led to the demise of the most extreme hypercalcifiers among the bivalves of the
404 lithiotid fauna (Trecalli et al., 2012). The same pattern of selective extinction of extreme
405 hypercalcifiers has been inferred for the extinction at the Permian–Triassic boundary (Knoll et al.,
406 2007) and for other events for which a claim has been made for ocean acidification (Kiessling and
407 Simpson, 2011; Honisch et al., 2012). Among the three survivors, *Gervilleioperna* and *Mytiloperna*
408 had less specialized and smaller shells (Accorsi Benini and Broglio Loriga, 1982; Broglio Loriga
409 and Posenato, 1995), which probably entailed a greater tolerance towards fluctuations of trophic
410 resources and reductions of the carbonate saturation state. *Opisoma* had a different life habit, being
411 an epifaunal edgewise recliner (Aberhan and von Hillebrandt, 1999; Posenato et al., 2014).
412
413 **6. Conclusions**
414

The Lower Jurassic sedimentary succession of the Maiellaro Quarry (Apennine Carbonate Platform) records the appearance, flourishing and demise of lithiotid bivalves. These three ecological evolutionary steps are documented by changes in the shell abundance, shell size and fabric of the lithiotid bivalve accumulations. Bio- and isotope stratigraphy indicate that, in the ACP, the lithiotid bivalves appeared during the late Pliensbachian. They rapidly became the dominating shallow-water carbonate components, together with the dasycladalean green alga *Palaeodasycladus mediterraneus*.

Although the bivalves occur in hard indurated limestones, the quality of the outcrop exposure in the Maiellaro quarry permitted their taxonomic identification at the genus level by means of diagnostic shell sections exposed on the fresh rock surface. Taxonomic identification allowed a more detailed comparison with the classical outcrops of the Rotzo Formation (Trento Platform). The lithiotid accumulations of the Maiellaro Quarry are dominated by *Cochlearites* and *Mytiloperna*, associated with subordinate *Lithioperna*. The great abundance of *Mytiloperna* and dasycladalean algae suggests that the shell beds developed in very shallow marine conditions. Another major peculiarity of the studied ACP lithiotid accumulations is the absence of bivalve mounds, which are instead common in the Trento Platform. The presence of exclusively tabular biostromes suggests a more regular and flat morphology of the platform top, probably linked to a lower subsidence rate. These factors could also explain why the ACP was able to remain in shallow-water conditions while many other platforms in the Tethyan area drowned during the early Toarcian.

The sudden demise of the lithiotid bivalves and of the dasycladalean algae occurred during the early Toarcian, at the onset of the negative T-OAE carbon isotope excursion associated. Their demise has been related to the physiological stress imposed by ocean acidification (Trecalli et al., 2012). The demise is preceded in the earliest Toarcian by a decrease of the rock-building contribution of the lithiotid bivalves, recorded as a drop in shell packing, maximum shell size and frequency of articulated shells. Repeated subaerial exposure during a sequence boundary

interval, coupled with accelerated weathering and increased nutrient input driven by global warming related to the P-To boundary event, could have concurred in creating environmental conditions less favourable to the lithiotid bivalves.

Acknowledgements

We are grateful to the Maiellaro quarry owners and to Dr. Italo Giulivo (Regione Campania) and his staff for facilitating our access. RP and DB have been supported by local research funds at the University of Ferrara (FAR 2014-17; FIR 2016). MP was supported by funds MIUR-PRIN 2010-11 (prot. 2010X3PP8J).

455 **References**

456

457 Aberhan, M., Hillebrandt, von A., 1996. Taxonomy, ecology, and palaeobiogeography of
458 *Gervilleioperna* (*Gervilleiognoma*) *aurita* n. subgen. n. sp. (Bivalvia) from the Middle Jurassic
459 of northern Chile. Paläontol. Z. 70, 79–96.

460 Aberhan, M., Hillebrandt, von A., 1999. The bivalve *Opisoma* in the Lower Jurassic of northern
461 Chile. Profil 16, 149–164.

462 Accorsi Benini, C., 1979. *Lithioperna*, un nuovo genere fra i grandi Lamellibranchi della facies a
463 "*Lithiotis*". Morfologia, tassonomia e analisi morfofunzionale. Boll. Soc. Paleontol. It. 18, 221–
464 257.

465 Accorsi Benini, C., Broglio Loriga, C., 1977. *Lithiotis* Gümbel, 1871 e *Cochlearites* Reis, 1903. I -
466 Revisione morfologica e tassonomica. Boll. Soc. Paleontol. It. 16, 15–60.

467 Accorsi Benini, C., Broglio Loriga, C., 1982. Microstrutture, modalità di accrescimento e
468 periodicità nei lamellibranchi liassici (Facies a '*Lithiotis'*). Geol. Rom. 21, 795–823.

469 Allison, P.A., Wignall, P.B., Brett, C.E., 1995. Palaeo-oxygenation: effects and recognition. In:
470 Bosence, D.J.W., Allison, P.A. (Eds.), Marine palaeoenviornmental analysis from fossils. Spec.
471 Publ. Geol. Soc. London 83, pp. 97–112,

472 Bassoullet, J.P., Baudin, F., 1994. Le Toarcien infeérieur: une période de crise dans les bassins et
473 sur les plate-formes carbonatées de l'Europe du Nord-Ouest et de la Téthys. Geobios 17, 645–
474 654.

475 Bassoullet, J.-P., Elmi S., Poisson A., Cecca F., Belion Y., Guiraud R. and Baudin F., 1993. Mid
476 Toarcian. In: J. Dercourt et al. (Eds.), Atlas Tethys Paleoenvironmental Maps. Becip-Franlab,
477 Rueil-Malmaison, France, pp. 63 – 80.

478 Berti Cavicchi, A., Bosellini, A., Broglio Loriga, C., 1971. Calcari a *Lithiotis problematica* o
479 Calcari a "Lithiotis"? Mem. Geopaleontol. Univ. Ferrara 3 (1), 41–53.

480 Blomeier, D.P.G., Reijmer, J.J.G., 1999. Drowning of a Lower Jurassic carbonate platform: Jbel
481 bou Dahar, High Atlas, Morocco. Facies 41, 81–110.
482 Bodin, S., Mattioli, E., Fröhlich, S., Marshall, J.D., Boutib, L., Lahsini, S., Redfern, J., 2010.
483 Toarcian carbon isotope shifts and nutrient changes from the Northern margin of Gondwana
484 (High Atlas, Morocco, Jurassic): palaeoenvironmental implications. Palaeogeogr.
485 Palaeoclimatol. Palaeoecol. 297, 377–390.
486 Bonardi G., D'Argenio B., Perrone V., 1988. Carta Geologica dell'Appennino meridionale. Mem.
487 Soc. Geol. It. 41, 1341.
488 Bosellini, A., 1972. Paleoecologia dei Calcari a "Lithiotis" (Giurassico inferiore, Prealpi Venete).
489 Riv. Ital. Paleontol. Stratigr. 78, 49–56.
490 Bosellini, A., 2004. The Western passive margin of Adria and its carbonate platforms. Spec. Vol. It.
491 Geol. Soc. 32nd Int. Geol. Congr., Florence, 20–28 August 2004, 79–92.
492 Broglio Loriga, C., Neri, C., 1976. Aspetti paleobiologici e paleogeografici della facies a "Lithiotis"
493 (Giurese inf.). Riv. Ital. Paleontol. Stratigr. 82, 651–706.
494 Broglio Loriga, C., Posenato, R., 1996. Adaptive strategies of Lower Jurassic and Eocene
495 multivincular bivalves. Boll. Soc. Paleontol. Ital., Spec. Vol. 3, 45–61.
496 Caswell, B.A., Coe, A.L., 2013. Primary productivity controls on opportunistic bivalves during
497 Early Jurassic oceanic deoxygenation. Geology 41 (11), 1163–1166.
498 Caswell, B.A., Coe, A.L., 2014. The impact of anoxia on pelagic macrofauna during the Toarcian
499 Oceanic Anoxic Event (Early Jurassic). Proc. Geol. Ass., 125(4), 383–391.
500 Catenacci, E., De Castro, P., Sgrosso, I., 1963. Complessi-guida del Mesozoico calcareo-dolomitico
501 nella zona orientale del Massiccio del Matese. Mem. Soc. Geol. Ital. 4, pp. 20.
502 Chinzei, K., 1982. Morphological and structural adaptations to soft substrates in the Early Jurassic
503 monomyarians *Lithiotis* and *Cochlearites*. Lethaia 15, 179–197.
504 Cohen, A.S., Coe, A.L., Harding, S.M., Schwark, L., 2004. Osmium isotope evidence for the
505 regulation of atmospheric CO_2 by continental weathering. Geology 32, 157–160.

De Castro, P., 1962. Il Giura-Lias dei Monti Lattari e dei rilievi ad Ovest della Valle dell'Irno e della Piana di Montoro. Boll. Soc. Natural. Napoli 71, 21–52.

Debeljak, I., Buser, S., 1998. Lithiotid bivalves in Slovenia and their mode of life. Geologija 40, 11–64.

Dera, G., Pellenard, P., Neige, P., Deconinck, J.-F., Puce at, E., Dommergues, J.-L., 2009. Distribution of clay minerals in Early Jurassic Peritethyan seas: palaeoclimatic significance inferred from multiproxy comparisons. Palaeogeogr. Palaeoclimatol. Palaeoecol. 271, 39–51.

Franceschi, M., Dal Corso, J., Posenato, R., Roghi, G., Masetti, D., Jenkyns, H.C., 2014. Early Pliensbachian (Early Jurassic) C-isotope perturbation and the diffusion of the *Lithiotis* Fauna: insights from the western Tethys. Palaeogeogr. Palaeoclimatol. Palaeoecol. 410, 255–263.

Fraser, N.M., Bottjer, D.J., Fischer, A.F., 2004. Dissecting "*Lithiotis*" Bivalves: implications for the Early Jurassic Reef Eclipse. Palaios 19, 51–67.

Fugagnoli, A., 2004. Trophic regimes of benthic foraminiferal assemblages in Lower Jurassic shallow water carbonates from northeastern Italy (Calcari Grigi, Trento Platform, Venetian Prealps). Palaeogeogr. Palaeoclimatol. Palaeoecol. 205, 111–130.

Geyer, O.F., 1977. Die "*Lithiotis*-Kalke" im Bereich der unterjurassischen Tethys. Neues Jahrb. für Geol. Paläontol. Abh. 153 (3), 304–340.

Gümbel, C.W., 1871. Die sogenannten Nulliporcn (*Lithothamnium* und *Dactylopora*) und ihre Betheiligung an der Zusammensetzung der Kalkgesteine. 1. Die Nulliporen des Pflanzenreichs (*Lithothamnium*). Anhang, *Lithiotis problematica*. Abh. Ak. Wiss. Münich. Cl. 2, 38–41.

Harries, P., Little, C., 1999. The early Toarcian (Early Jurassic) and the Cenomanian–Turonian (Late Cretaceous) mass extinctions: similarities and contrasts. Palaeogeogr. Palaeoclimatol. Palaeoecol. 154, 39–66.

Hauser, I., Oschmann, W., Gischler, E., 2008, Taphonomic signatures on modern Caribbean bivalve shells as indicators of environmental conditions (Belize, central America). Palaios 23, 586–600.

Hermoso, M., Minoletti, F., Rickaby, R. E. M., Hesselbo, S. P., Baudin, F., & Jenkyns, H. C., 2012. Dynamics of a stepped carbon-isotope excursion: Ultra high-resolution study of Early Toarcian environmental change. Earth Planet. Sci. Lett. 319, 45–54.

Hesselbo, S.P., Gröcke, D.R., Jenkyns, H.C., Bjerrum, C.J., Farrimond, P., Morgans Bell, H.S., Green, O.R., 2000. Massive dissociation of gas hydrate during a Jurassic oceanic anoxic event. Nature 406, 392–395.

Hesselbo, S.P., Jenkyns, H.C., Duarte, L.V., Oliveira, L.C.V., 2007. Carbon-isotope record of the Early Jurassic (Toarcian) Oceanic Anoxic Event from fossil wood and marine carbonate (Lusitanian Basin, Portugal). Earth Planet. Sci. Lett. 253, 455–470.

Hönisch, B., Ridgwell, A., Schmidt, D.N., Thomas, E., Gibbs, S.J., Sluijs, A., Zeebe, R., Kump, L., et al., 2012. The geological record of ocean acidification. Science 335, 1058–1063.

Jenkyns, H.C., 1988. The early Toarcian (Jurassic) event: stratigraphy, sedimentary, and geochemical evidence. Am. J. Sci. 288, 101–151.

Jenkyns, H., 2003. Evidence for rapid climate change in the Mesozoic–Palaeogene greenhouse world. Phil. Trans. R. Soc. A: Math., Phys. Eng. Sci. 361(1810), 1885–1916.

Knoll, A.H., Bambach, R.K., Payne, J., Pruss, S., Fischer, W., 2007. A paleophysiolo- gical perspective on the end-Permian mass extinction and its aftermath. Earth Planet. Sci. Lett. 256, 295–313.

Kidwell, S.M., Holland, S.M. 1991. Field description of coarse bioclastic fabrics. Palaios 6, 426–434.

Kiessling, W., Simpson, C., 2011. On the potential for ocean acidification to be a general cause of ancient reef crises. Global Change Biol. 17, 56–67.

Krencker, F.-N., Bodin, S., Suan, G., Heimhofer, U., Kabiri, L., Immenhauser, A., 2015. Toarcian extreme warmth led to tropical cyclone intensification. Earth Planet. Sci. Lett. 425, 120–130.

555 Leinfelder, R., Schmid, D.U., Nose, M., Werner, W., 2002. Jurassic reef patterns - the expression of
556 a changing globe. In: Kiessling, W., Flügel, E., Golonka, J. (Eds.), Phanerozoic Reef Patterns.
557 SEPM Spec. Pub. 72, 465–520.
558 Léonide, P., Floquet, M., Durlet, C., Baudin, F., Pittet, B., Lécuyer, C., 2012. Drowning of a
559 carbonate platform as a precursor stage of the Early Toarcian global anoxic event (Southern
560 Provence sub-Basin, South-east France). Sedimentology 59, 156–184.
561 Littler, K., Hesselbo, S. P., & Jenkyns, H. C., 2010. A carbon-isotope perturbation at the
562 Pliensbachian-Toarcian boundary: evidence from the Lias Group, NE England. Geol. Mag.
563 147(2), 181–192.
564 Morten, S.D., Twitchett, R.J., 2009. Fluctuations in the body size of marine invertebrates through
565 the Pliensbachian–Toarcian extinction event. Palaeogeogr. Palaeoclimatol. Palaeoecol. 284,
566 29–38.
567 Pálfy, J., Smith, P., 2000. Synchrony between Early Jurassic extinction, oceanic anoxic event, and
568 the Karoo-Ferrar flood basalt volcanism. Geology 28, 747–750.
569 Posenato R., Bassi D., Nebelsick J., 2013. *Opisoma excavatum* Bohem, a Lower Jurassic alatoform
570 chambered bivalve. Lethaia 46, 242–437.
571 Posenato, R., Masetti, D., 2012. Environmental control and dynamics of Lower Jurassic bivalve
572 build-ups in the Trento Platform (Southern Alps, Italy). Palaeogeogr. Palaeoclimatol.
573 Palaeoecol. 361–362, 1–13.
574 Reis, O., 1903. Über Lithiotiden. Abh. K.-K. Geol. Reich. 17 (6), 1–44.
575 Sabatino, N., Vlahovic, I., Jenkyns, H.C., Scopelliti, G., Neri, R., Prtoljan, B., Velc, I., 2013.
576 Carbon-isotope record and palaeoenvironmental changes during the early Toarcian oceanic
577 anoxic event in shallow-marine carbonates of the Adriatic Carbonate Platform in Croatia. Geol.
578 Mag. 150, 1085–1102.
579 Scheibner C., Reijmer J.J.G., 1999. Facies patterns within a Lower Jurassic upper slope to inner
580 platform transect (Jbel Bou Dahar, Morocco). Facies, 41, 55–80.

581 Seilacher, A., 1984. Constructional morphology of bivalves evolutionary pathways in primary
582 versus secondary soft dwellers. Palaeontology 27 (2), 207–237.
583 Strasser, A., 1988. Shallowing-upward sequences in Purbeckian peritidal carbo- nates (lowermost
584 Cretaceous, Swiss and French Jura Mountains). Sedimentology 35, 369–383.
585 Strasser, A., Hillgärtner, H., Hug, W., Pittet, B., 2000. Third-order depositional sequences resulting
586 from Milankovitch cycles. Terra Nova 12, 303–311.
587 Suan, G., Mattioli, E., Pittet, B., Lécuyer, C., Suchéras-Marx, B., Duarte, L. V., Philippe, M.,
588 Reggiani, L., Martineau, F., 2010. Secular environmental precursors to Early Toarcian
589 (Jurassic) extreme climate changes. Earth Planet. Sci. Lett. 290(3-4), 448–458.
590 Trecalli, A., Spangenberg J., Adatte T., Föllmi K.B., Parente M., 2012. Carbonate platform
591 evidence of ocean acidification at the onset of the early Toarcian oceanic event. Earth Planet.
592 Sci. Lett. 357–358, 214–225.
593 Twitchett, R.J., 2007. The Lilliput affect in the aftermath of the end-Permian extinction event.
594 Palaeogeogr. Palaeoclimatol. Palaeoecol. 252, 132–144.
595 Urbanek A., 1993. Biotic crises in the history of Upper Silurian graptoloids: a palaeobiological
596 model. Hist. Biol. 7, 29–50.
597 Wignall, P.B., Newton, R.J., Little, C.T.S., 2005. The timing of paleoenvironmental change and
598 cause-and-effect relationships during the early Jurassic mass extinction in Europe. Am. J. Sci.
599 305, 1014–1032.
600 Wilmsen, M., Neuweiler, F., 2008. Biosedimentology of the Early Jurassic post- extinction
601 carbonate depositional system, central High Atlas rift basin, Morocco. Sedimentology 55, 773–
602 807.
603 Woodfine, R.G., Jenkyns, H.C., Sarti, M., Baroncini, F., Violante, C., 2008. The response of two
604 Tethyan carbonate platforms to the early Toarcian (Jurassic) oceanic anoxic event:
605 environmental change and different subsidence. Sedimentology 55, 1011–1028.

606 Yin, J., Fürsich, F.T., 1991. Middle and Upper Jurassic bivalves from the Tanggula Mountains, W-
607 China. Beringeria Würzb. geowiss. Mitt. 4, 127–192.
608
609
610
611
612
613
614
615
616
617
618
619
620
621
622
623
624
625
626
627
628
629
630
631

632 **Figure captions**

633

634 **Fig. 1.** Toarcian palaeogeography of the peri-Tethyan domains (redrawn from Bassoullet et al.,
635 1993) with location of the studied area, the Apennine Carbonate Platform (ACP) of southern
636 Italy, and of the classical lithiotid localities of the Trento Carbonate Platform (TCP).

637

638 **Fig. 2.** Schematic geological map of the central-southern Apennines with location of the studied
639 section (modified from Bonardi et al., 1988).

640

641 **Fig. 3.** The Maiellaro quarry at Mercato San Severino (Salerno, southern Italy). The Lower Jurassic
642 of the ACP comprises the *Palaeodasycladus* Limestones Formation, overlain by the Oolitic-
643 oncolitic Limestomes Formation. The upper part of the *Palaeodasycladus* Limestones
644 Formation, called the *Lithiotis* Member, is characterized by the abundant occurrence of lithiotid
645 bivalves, which make metre-thick, bed-parallel shell accumulations. A–D, the four
646 distinguished tapho-horizons of lithiotid accumulations.

647

648 **Fig. 4.** Stratigraphic log of the *Lithiotis* Member and the lowermost part of the Oolitic-oncolitic
649 Limestones Formation in the Maiellaro Quarry (Mercato San Severino, Salerno). The boxes
650 indicate the position and thickness of the bivalve accumulations (Biv. acc.). Four tapho-
651 horizons (A–D) were distinguished based on the shell fabric and taphonomic characters of the
652 lithiotid accumulation (see text). The tentative position of the Piensbachian–Toarcian boundary
653 (?Pl-To) is after the isotope stratigraphy of Trecalli et al. (2012); other symbols: L-O, *Lithiotis*
654 Member and Oolitic-oncolitic Limestones boundary; O-o Lms, Oolitic-oncolitic Limestones;

655

656 **Fig. 5.** Field examples of the applied semi-quantitative method to assess the PI, AI and FI value
657 combinations. (A) Oolitic-oncolitic Limestones Formation, tapho-horizon D. (B) *Lithiotis*

Member, tapho-horizon A. (C) *Lithiotis* Member, tapho-horizon B. (D) *Lithiotis* Member, tapho-horizon B. (E) *Lithiotis* Member, tapho-horizon B. (F) *Lithiotis* Member, tapho-horizon B. Further details in the text.

Fig. 6. (A) Densely packed bivalve accumulation dominated by *Lithioperna* in life position (lower part of tapho-horizon B). (B) Detail of the former accumulation. (C) Articulated shells of *Mytiloperna* in life position (tapho-horizon C). (D) A bouquet-like aggregation of large *Cochlearites* shells in life position (tapho-horizon B). (E) Sparse accumulation of *Lithioperna* (tapho-horizon C). (F) Fragmented and possibly reworked *Lithiotis* shells (tapho-horizon D, lowermost part of the Oolitic-oncolitic Limestones Formation). (G) Articulated shell of a megalodontid (tapho-horizon B). (H) Articulated shells of *Mytiloperna* and *Lithioperna* (tapho-horizon A). (I) Articulated shells of *Lithioperna* (tapho-horizon B). (J) Articulated shells of *Cochlearites* (tapho-horizon B). (K) *Opisoma* (tapho-horizon A). Scale bars represent 5 cm.

Fig. 7. Taxonomic composition and taphonomic characters of the bivalve shell beds in the Maiellaro Quarry are used to distinguish four tapho-horizon (A–D) (see text for an explanation of the taphonomic indexes). The carbon isotope profiles of Trecalli et al. (2012) are used to establish a chronostratigraphic framework and to highlight the position of the Pliensbachian–Toarcian boundary event and of the early Toarcian oceanic anoxic event. Coc, *Cochlearites*; ind, not classified bivalve; Lit, *Lithioperna*; Lts, *Lithiotis*; Meg, megalodontids; Myt, *Mytiloperna*; Opi, *Opisoma*; A–D, tapho-horizons; O.L., Oolitic-oncolitic Limestones Formation.

Fig. 8. Changes in taphonomic signatures of the bivalve accumulations through the four tapho-horizons (A–D) of the Maiellaro quarry succession. See the text for an explanation of the indexes.

684

685 **Fig. 9.** A detail of the last densely packed bivalve accumulation of the *Lithiotis* Member in the
686 Maiellaro Quarry (upper part of the tapho-horizon C). (A) *Mytiloperna* (Myt) and *Cochlearites*
687 (Coc) shells in life position. (B) A large shell, probably of *Cochlearites* (?Coc) and *Lithiotis*
688 like shells (?Lts) at the lower right corner.

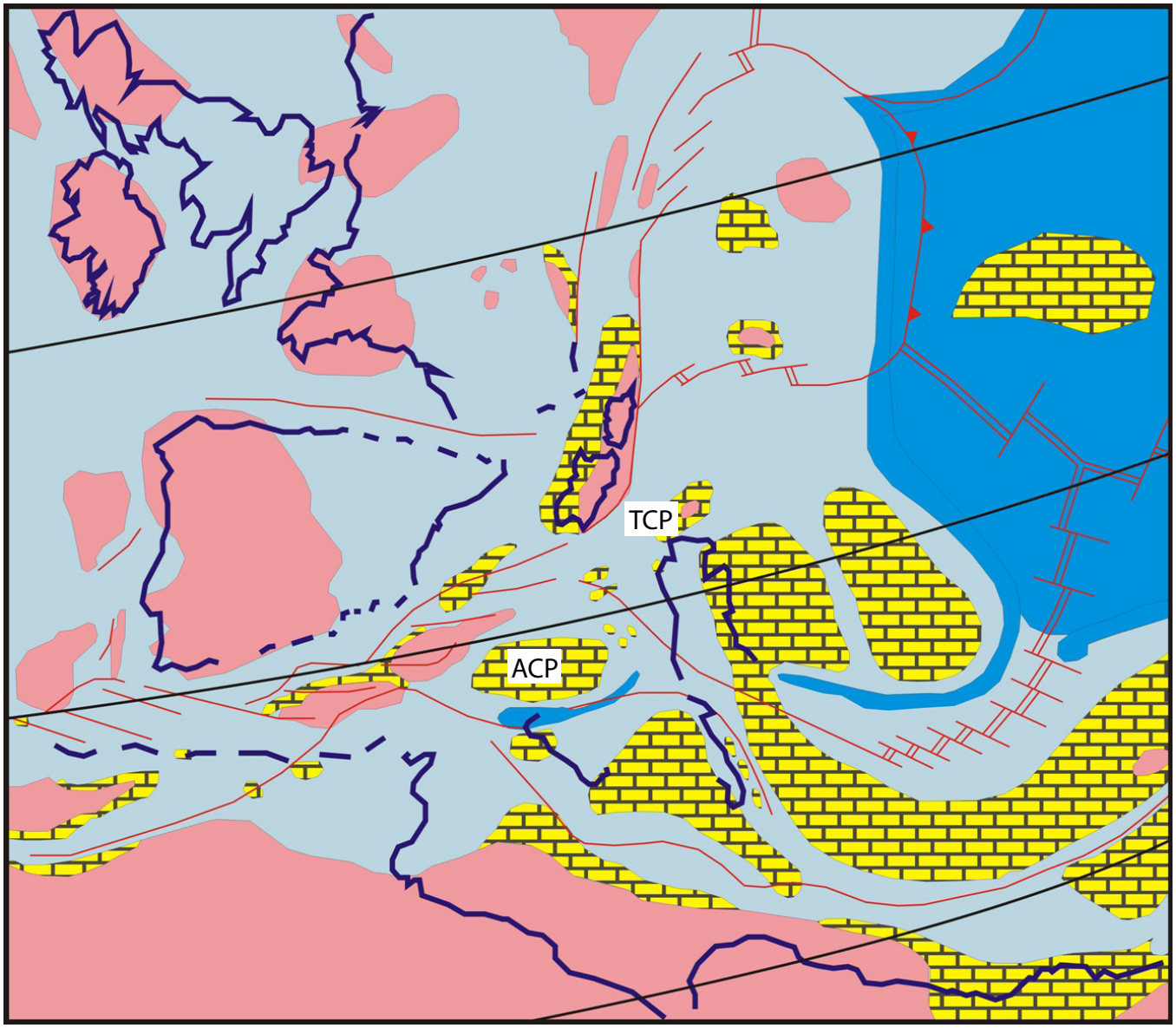

Posenato et al. Fig. 1

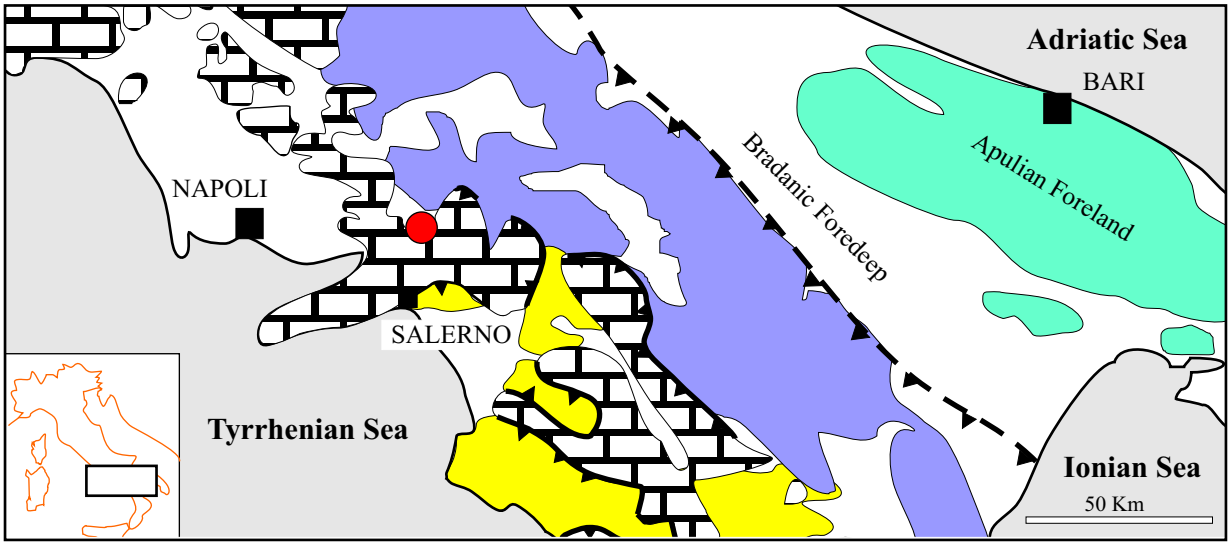
Adriatic Sea
BARI
Apulian Foreland
Bradanic Foredeep
NAPOLI
SALERNO
Tyrrhenian Sea
Ionian Sea
50 Km
Apennine Carbonate Platform
Lagonegro-Molise basinal units
Plio-Quaternary deposits and volcanics
Apulian Carbonate Platform
Ligurides and Sicilides units
Maiellaro quarry
Main thrust fronts
Main buried thrust fronts

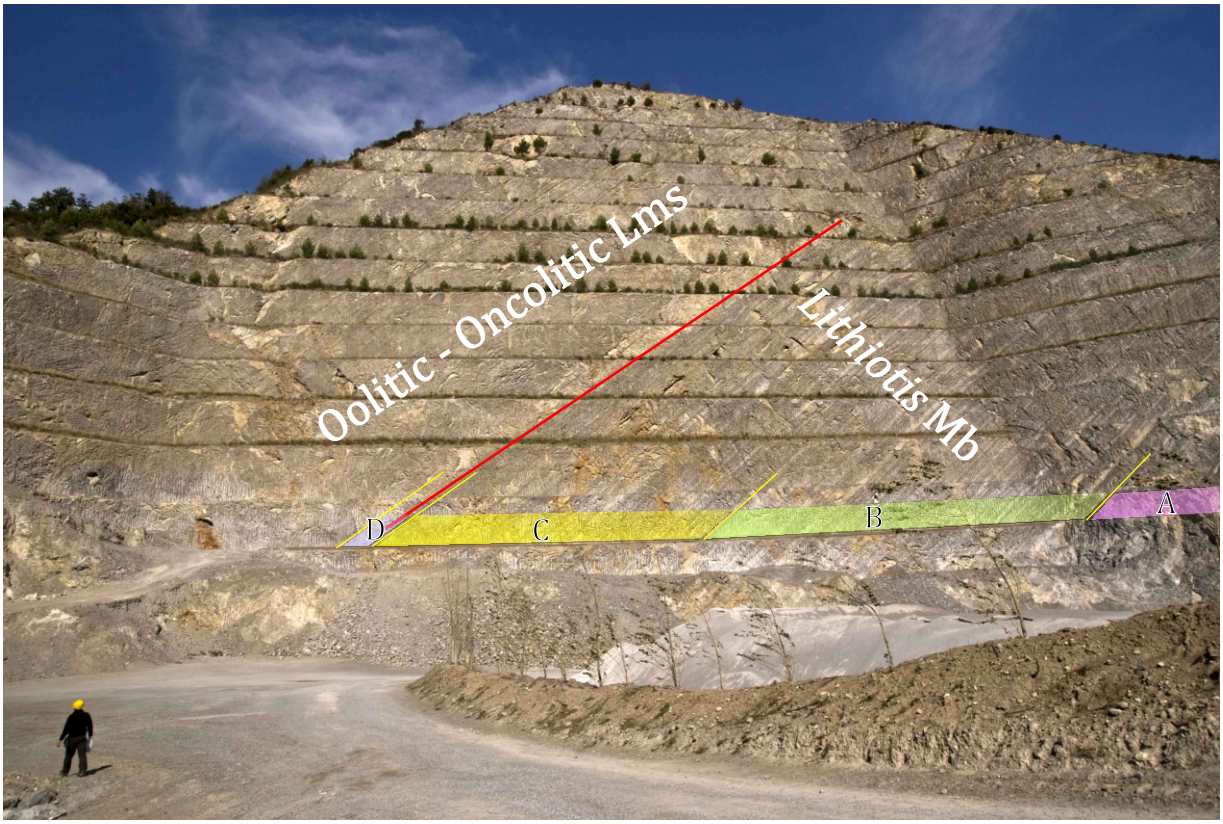

Posenato et al., Fig. 3

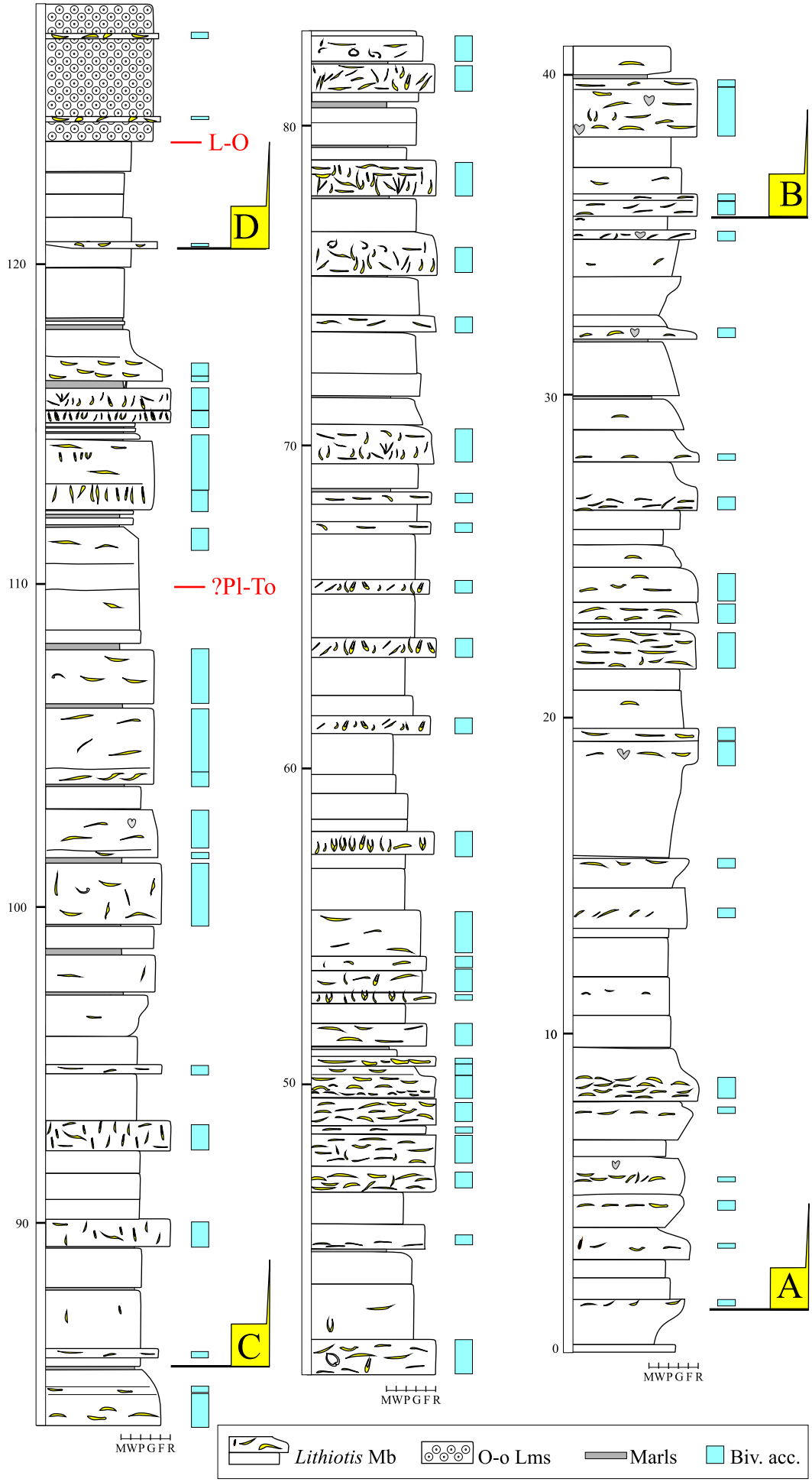

Posenato et al Fig. 4

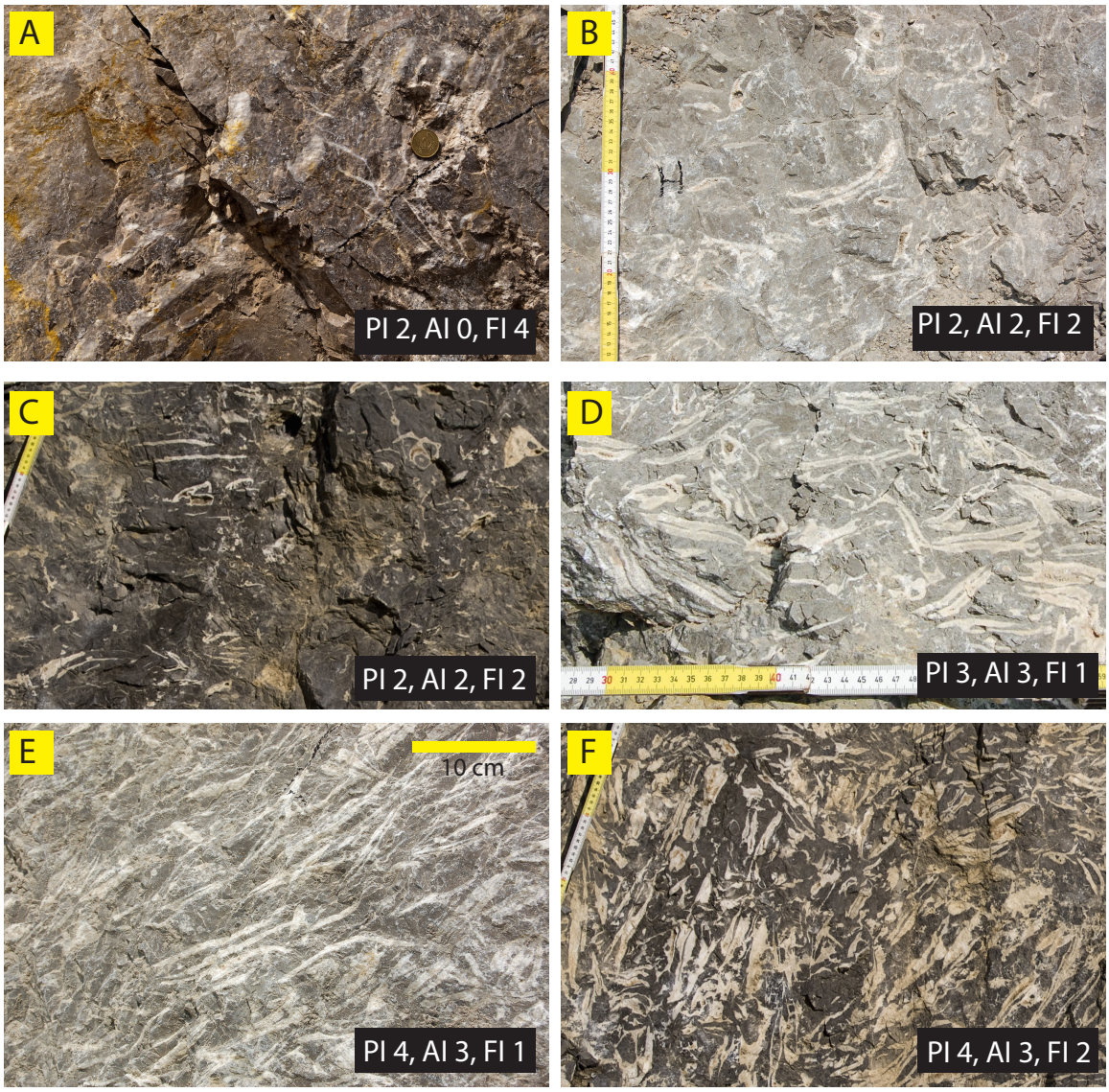

Posenato et al Fig. 5

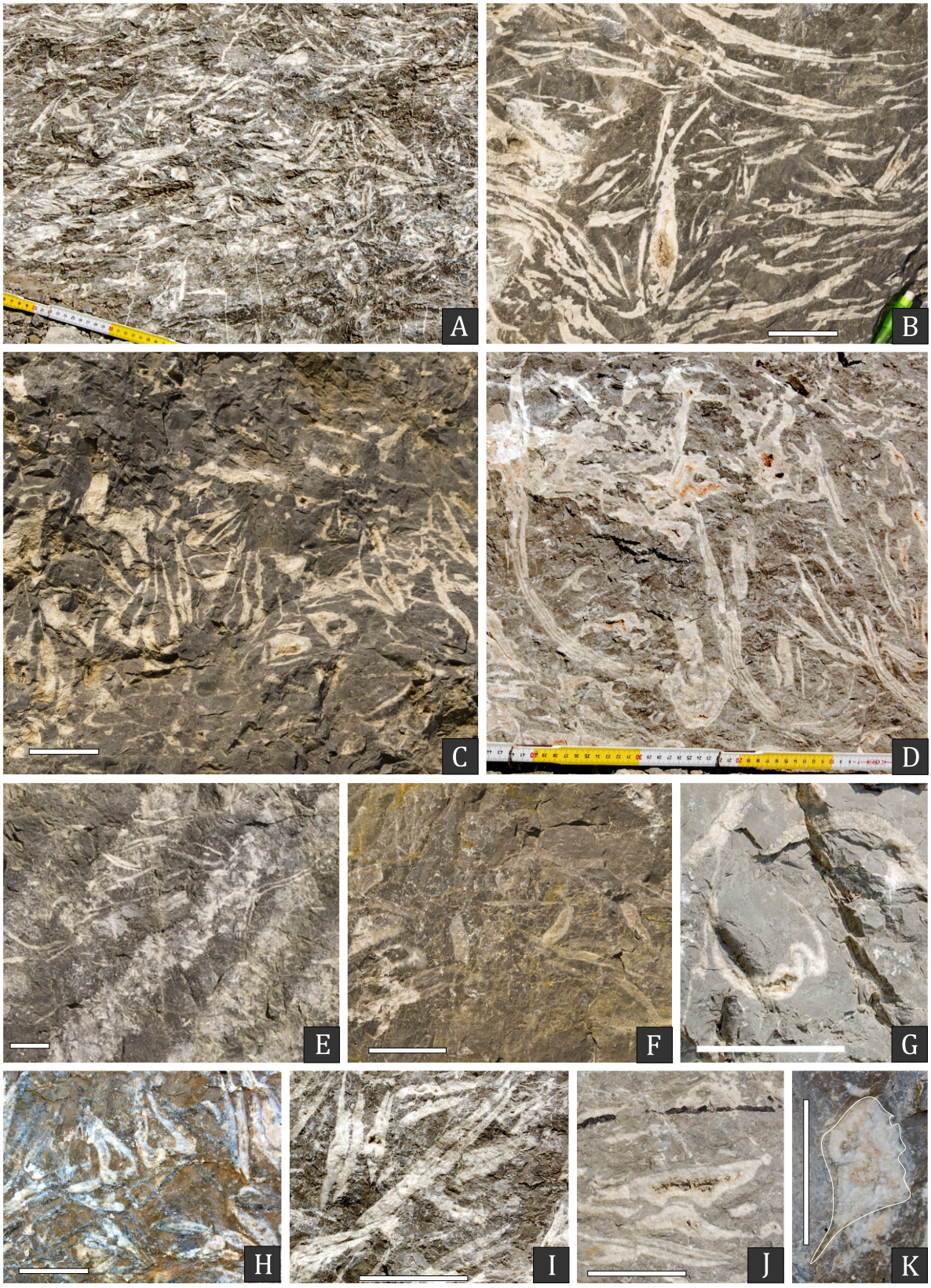

Posenato et al Fig. 6

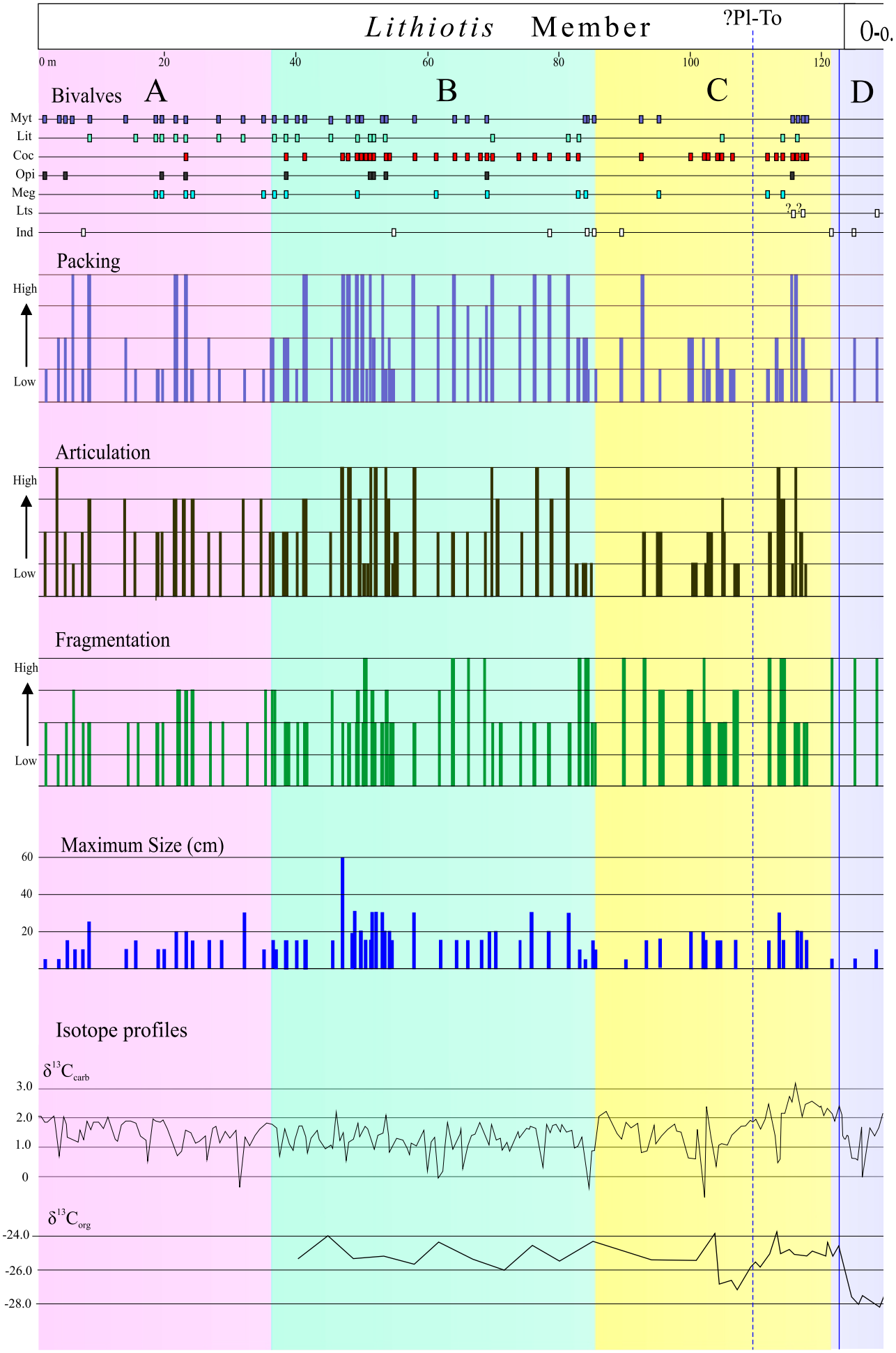

Posenato et al. Fig. 7

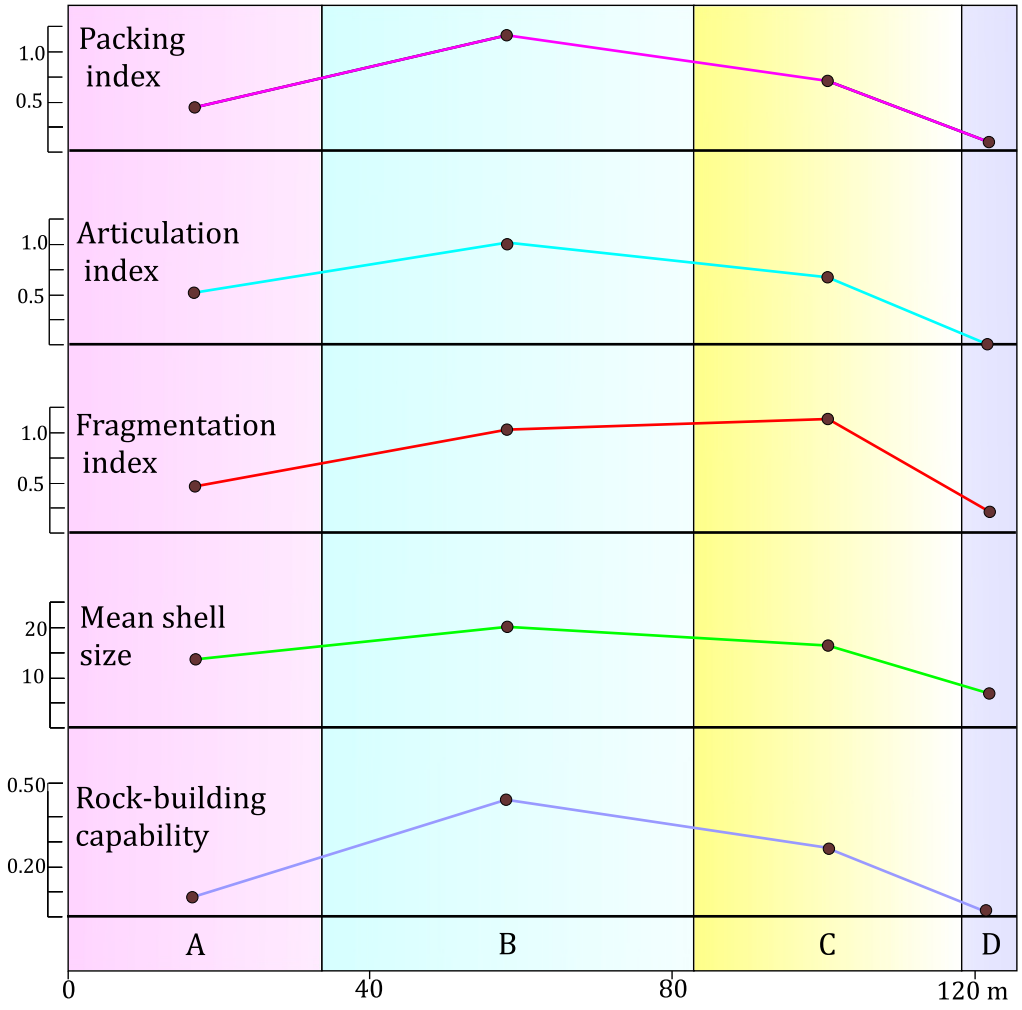

Posenato et al Fig. 8

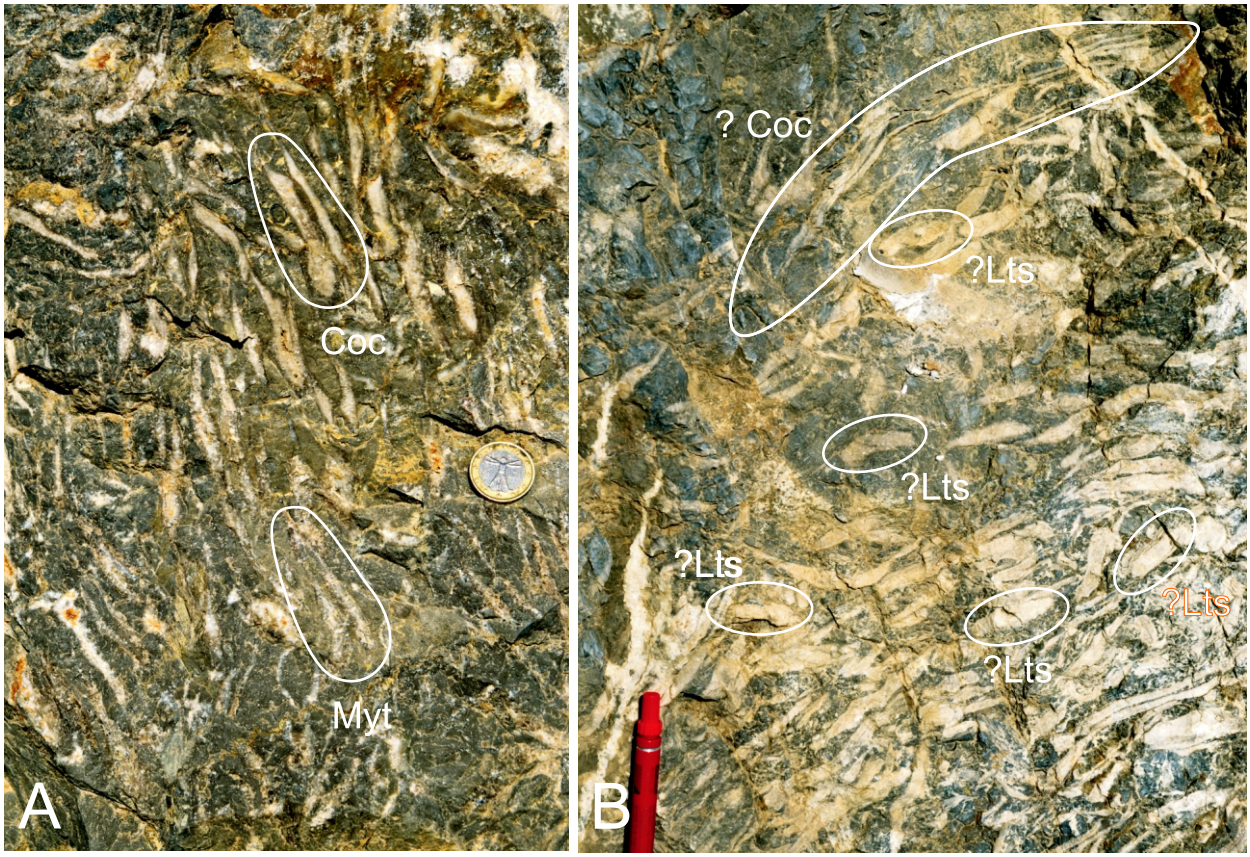

Posenato et al. Fig. 9

SUPPLEMENTARY MATERIAL

Table 1. Taphonomic parameters and taxonomic composition of the shell-beds of the Maiellaro Quarry succession. a, bed thickness (cm); b, shell-bed thickness; c, packing index; d, articulation index; e, fragmentation index; f, maximum shell size; g, shell-bed packing score (b × c); h, shell-bed articulation score (b × d); i, shell-bed fragmentation score (b × e); j, key to bivalve genera: Coc, *Cochlearites*; ind, undetermined bivalve; Lit, *Lithioperna*; Lts, *Lithiotis*; Meg, megalodontids; Myt, *Mytiloperna*; Opi, *Opisoma*.

Table 2. Summary of the taphonomic indexes used in this study for the distinguished tapho-horizons A–D. For each tapho-horizon a cumulative score is calculated for each parameter by summing the score of each-shell bed (see Tab. 1). Then, for each tapho-horizon, we calculated the horizon-averaged packing, articulation and fragmentation scores dividing the cumulative score by the total thickness of the horizon. The horizon-averaged packing score is used as a proxy of the rock-building contribution of the lithiotid bivalves, because this score embodies information on the abundance of lithiotid shell relative to the total volume of the rock.

a	b	c	d	e	f	g	h	i	j
20	20	2	0	4	10	40	0	80	Lts
260		0	0	0					
10	10	2	0	4	5	20	0	40	ind
350		0	0	0					
10	10	1	0	4	5	10	0	40	ind
80		0	0	0	0				
730	**40**				**10**	**70**	**0**	**160**	**tapho-hor. D**
90		0	0	0					
200		0	0	0					
40	40	1	1	2	15	40	40	80	Myt, Coc
20	20	2	1	2	20	40	20	40	Myt , Coc
35		0	0	0					
65	65	4	2	2	30	260	130	130	Myt, Coc, ?Lts
50	50	4	4	2	20	200	200	100	Myt Coc Opi
40		0	0	0					
170	170	1	1	4	15	170	170	680	Coc, Meg
60	60	2	4	2	30	120	240	120	Coc
50		0	0	0					
70	70	1	2	4	15	70	140	280	Coc, Meg, ?Lts
20		0	0	0					
130		0	0	0					
180		0	0	0					
190	190	1	1	3	15	190	190	570	Coc
10		0	0	0					
200	200	1	2	2	15	200	400	400	Coc
50	50	2	3	2	15	100	150	100	Coc
40		0	0	0					
120	120	1	2	2	15	120	240	240	Coc
20	20	2	1	4	20	40	20	80	Coc
20		0	0	0					
200	200	2	1	3	20	400	200	600	Coc
75		0	0	0					
90		0	0	0					
60		0	0	0					
210		0	0	0					
30	30	1	2	3	15	30	60	90	Myt, Meg
180		0	0	0					
80	80	4	2	4	15	320	160	320	Myt, Coc
210		0	0	0					
80	80	2	0	4	5	160	0	320	ind
80		0	0	0					
120		0	0	0					
210		0	0	0					
20	20	1	0	2	10	20	0	40	Myt Ind
30		0	0	0					
3545	**1465**				**30**	**2480**	**2360**	**4190**	**tapho-hor. C**
20	20	1	1	2	15	20	20	40	Myt Ind
110	110	2	1	4	5	220	110	440	Myt, Meg
20		0	0	0					
90	90	2	1	4	10	180	90	360	Coc, Meg
20		0	0	0					
80	80	4	4	2	30	320	320	160	Coc
120		0	0	0					
100		0	0	0					
100	100	4	3	2	20	400	300	200	Coc Ind
160		0	0	0					
80	80	4	4	2	30	320	320	160	Coc
150		0	0	0					
50	50	3	2	2	15	150	100	100	Coc

180		0	0	0					
30		0	0	0					
90		0	0	0					
100	100	4	3	2	20	400	300	200	Lit, Coc
100		0	0	0					
30	30	3	4	2	20	90	120	60	Myt, Coc, Opi, Meg
60		0	0	0					
30	30	2	2	4	15	60	60	120	Coc
160		0	0	0					
40	40	3	2	4	15	120	80	160	Myt, Coc
140		0	0	0					
60	60	4	2	4	15	240	120	240	Myt, Coc
125		0	0	0					
75		0	0	0					
50	50	3	2	3	15	150	100	150	Coc, Meg
300		0	0	0					
80	80	4	4	2	30	320	320	160	Myt, Coc
10		0	0	0					
185		0	0	0					
130	130	1	2	2	15	130	260	260	ind
30	30	2	1	1	20	60	30	30	Coc
80	80	1	3	3	20	80	240	240	Myt, Lith, Coc, Opi
15	15	4	4	2	30	60	60	30	Myt
80		0	0	0					
70	70	2	4	2	30	140	280	140	Lit, Coc, Opi
50		0	0	0					
10	10	4	4	1	30	40	40	10	Lit, Coc, Opi
30	30	1	1	3	15	30	30	90	Coc
80	80	4	1	4	15	320	80	320	Myt, Coc
25		0	0	0					
60	60	4	3	3	20	240	180	180	Myt, Lit, Coc, Meg
20	20	1	0	2	20	20		40	Coc
100	100	4	4	2	30	400	400	200	Coc, Myt
30		0	0	0					
50	50	4	4	2	60	200	200	100	Coc
150		0	0	0					
30	30	2	2	3	15	60	60	90	Myt, Lit
10		0	0	0					
280		0	0	0					
110	110	4	3	2	15	440	330	220	Myt, Coc
110		0	0	0					
25	25	1	2	2	15	25	50	50	Myt Lit
160	160	2	2	2	15	320	320	320	Myt, Lit, Coc, Opi, Meg
90		0	0	0					
60		0	0	0					
30		0	0	0					
20	20	2	2	3	10	40	40	60	Myt, Lit, Meg
40	40	2	2	3	15	80	80	120	Myt, Lit, Meg
4920	**1980**				**60**	**5675**	**5040**	**5050**	tapho-hor. B
70		0	0	0					
30	30	1	3	3	10	30	90	90	Myt, Meg
80		0	0	0					
180		0	0	0					
30	30	1	3	2	30	30	90	60	Myt, Lith
80		0	0	0					
120		0	0	0					
60		0	0	0					
110		0	0	0					
20	20	1	2	2	15	20	40	40	Myt, Lith
110		0	0	0					
40	40	2	2	2	15	80	80	80	Myt, Lit

45		0	0	0					
75		0	0	0					
60		0	0	0					
85	85	1	3	3	15	85	255	255	Meg
25		0	0	0					
60	60	4	3	3	20	240	180	180	Myt, Lit, Coc, Opi, Meg
30		0	0	0					
110	110	4	3	3	20	440	330	330	Myt, Lit
110		0	0	0					
80		0	0	0					
40	40	1	2	2	10	40	80	80	Myt, Lit, Opi, Meg
75	75	1	2	2	10	75	150	150	Myt, Lit, Meg
30		0	0	0					
155		0	0	0					
100		0	0	0					
30	30	1	2	2	15	30	60	60	Lit
125		0	0	0					
30	30	2	3	2	10	60	90	60	Myt
125		0	0	0					
110		0	0	0					
105		0	0	0					
120		0	0	0					
35		0	0	0					
65	65	4	3	2	25	260	195	130	Myt, Lit
75		0	0	0					
20	20	1	2	2	10	20	40	40	Ind
135		0	0	0					
15	15	4	1	3	10	60	15	45	Myt
85		0	0	0					
30	30	2	2	2	15	60	60	60	Myt, Opi
95		0	0	0					
15	15	2	4	1	5	30	60	15	Myt
25		0	0	0					
75		0	0	0					
65		0	0	0					
20	20	1	2	2	5	20	40	40	Myt, Opi
145		0	0	0					
3555	**715**				30	**1580**	**1855**	**1715**	**tapho-hor. A**

a: bed thickness
b: shell-bed thickne
c: packing index
d: articulation index
e: fragmentation index
f: maximum shell siz
g: shell-bed packing score (c
h: shell-bed articulation score (d*b)
i: shell-bed fragmentation score (e*b)
j: taxonomic composition of shell-bed

Coc: Cochlearites
Lit: Lithioperna
Meg: Megalodontids
Myt: Mytiloperna
ind: undetermined bi
Opi: Opisoma
Lts: Lithiotis

	Tapho-horizons		A	B
a	Tapho-horizon thickness (cm)		3555	4920
b	cumulative thickness of shell beds (cm)		715	1980
c	cumulative packing score		1580	5675
d	horizon-averaged packing score	c/a	**0.44**	**1.15**
e	cumulative articulation score		1855	5040
f	horizon-averaged articulation score	e/a	**0.52**	**1.02**
g	cumulative fragmentation score		1715	5050
h	horizon-averaged fragmentation score	g/a	**0.48**	**1.03**
i	largest value of maximum shell size		30	60
j	mean value of maximum shell size		14	20

c = shell-bed thickness*packing index
e = shell-bed thickness*articulation index
g = shell-bed thickness*fragmentation index

C	D
3545	730
1465	40
2480	70
0.70	**0.10**
2360	0
0.67	**0.00**
4149	160
1.17	**0.22**
30	10
16	7